

Supplemental Material for

**First-principles based quantification of charged species redistribution at  
electrochemical interfaces: Model system of zirconium oxide**

Jing Yang<sup>1</sup>, Mostafa Youssef<sup>1,2,3</sup>, Bilge Yildiz<sup>1,2\*</sup>

<sup>1</sup>Laboratory for Electrochemical Interfaces, Department of Materials Science and Engineering, Massachusetts Institute of Technology, 77 Massachusetts Avenue, Cambridge, MA 02139, USA.

<sup>2</sup>Department of Nuclear Science and Engineering, Massachusetts Institute of Technology, 77 Massachusetts Avenue, Cambridge, MA 02139, USA.

<sup>3</sup>Department of Mechanical Engineering, The American University in Cairo, AUC Avenue, P.O. Box 74, New Cairo 11835, Egypt

\*Correspondence to: [byildiz@mit.edu](mailto:byildiz@mit.edu)

**List of contents:**

1. Hydrogen-rich and oxygen-rich conditions
2. Aligning the energy levels of water and ZrO<sub>2</sub>
3. Solution scheme of the continuum model
4. Bulk defect chemistry of doped ZrO<sub>2</sub>
5. Electrostatic profile of doped-ZrO<sub>2</sub>/water interface with varying pH
6. Effect of varying doping concentration

**1. Hydrogen-rich and oxygen-rich conditions**

We used the definition of hydrogen-rich and oxygen-rich conditions as in Ref. [1]. Under hydrogen-rich conditions ( $T^\circ = 298.15$  K,  $p_{H_2}^\circ = 1$  bar),  $\mu_H = 0$ . Under oxygen-rich conditions ( $T^\circ = 298.15$  K,  $p_{O_2}^\circ = 1$  bar),  $\mu_O = 0$ . The chemical potential of oxygen and hydrogen is connected by  $2\mu_H + \mu_O = \Delta G^\circ(H_2O)$ , which is -2.46 eV. It should be noted that changing the conditions from oxygen-rich to hydrogen-rich will

not change the pH - ion concentration diagram significantly given that water chemistry is mainly controlled by  $A^+$  and  $B^-$  extrinsic ions (for example,  $Na^+$  and  $Cl^-$  ions).

Throughout the manuscript we presented results at oxygen-rich condition. Here we reproduce Figure 3 and Figure 4 in the main article at hydrogen-rich condition. The major difference here is that under hydrogen-rich condition, the Fermi level of water solution at  $pH = 7$  rises from  $-5.5$  eV to  $-4.3$  eV (referenced to vacuum level). This change increases the Fermi level difference on the two sides and therefore the built-up potential is larger. Other than that, all qualitative conclusions do not change by much. The main reason why Fermi level difference change is qualitatively insignificant is that in both cases bulk defect/ion chemistry of water solution and  $ZrO_2$  does not change significantly with  $p_{O_2}$ . This determines the ionic strength on both sides and thus determines Debye length and how the potential drop is distributed on the two sides.

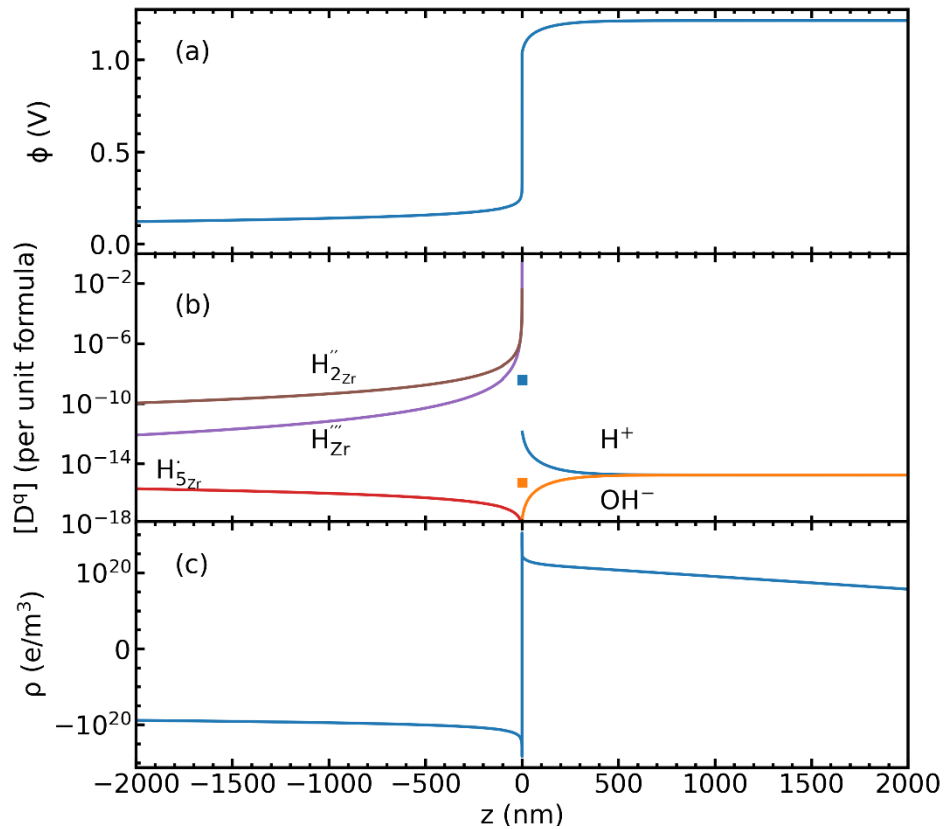


Figure S1. (a) Electrostatic potential  $\phi$ , (b) concentration of charged species, and (c) charge density  $\rho$  across  $ZrO_2$ /water interface at  $pH = 7$  hydrogen-rich condition. The interface is placed at  $z = 0$  with the left side being  $ZrO_2$  and the right side being water.

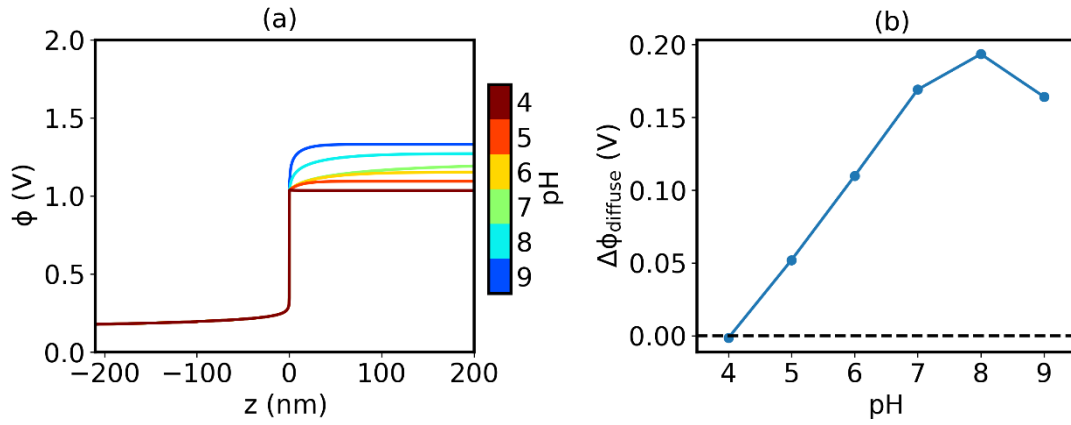


Figure S2. Reproducing Figure 4 in the main article under hydrogen rich condition. (a) the electrostatic potential profile with varying  $pH$  of water solution. (b) the potential drop in the diffuse layer  $\Delta\phi_{\text{diffuse}}$  as a function of  $pH$ . The point where the potential drop reaches zero corresponds to PZC.

## 2. Aligning the energy levels of water and $ZrO_2$

To align the energy levels of water and  $ZrO_2$ , we applied the universal hydrogen level method as described in [2]. The universal hydrogen level, as shown to align in semiconductors, insulators and solutions, is defined as the Fermi level at which  $H^+$  and  $H^-$  in the matrix have equal formation energy. In water, this level is the potential of standard hydrogen electrode (SHE) (-4.44 eV). We applied this method to find the hydrogen level in  $ZrO_2$ , as shown in Figure S3 (a). The Fermi level at which formation energy of  $H_i^\bullet$  and  $H_i'$  intersect is 2.83 eV above valence band maximum. Aligning this with water, we arrive at the band alignment profile in Figure S3 (b), where we find that the valence band maximum of water is 0.15 eV higher than the valence band of  $ZrO_2$ .

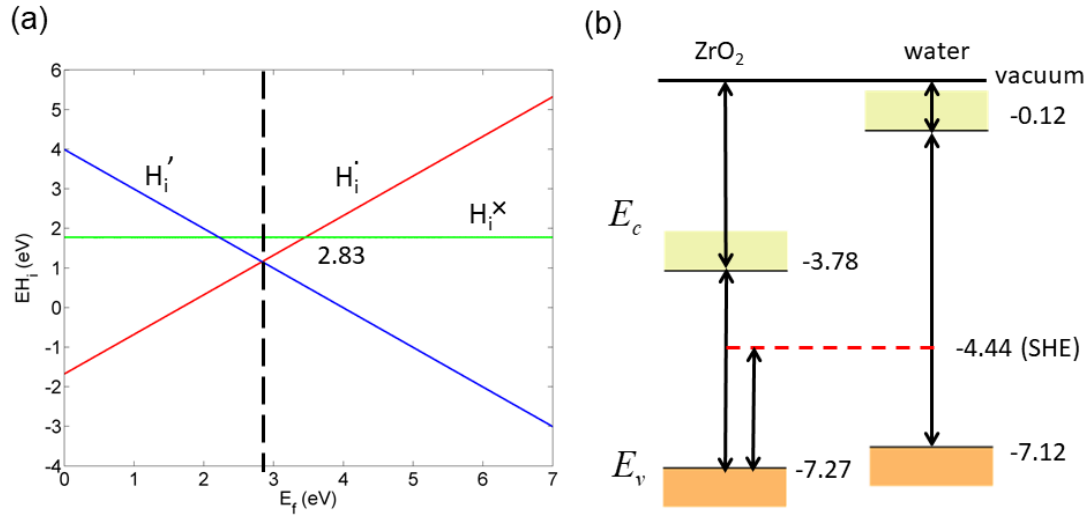


Figure S3. (a) Formation energy of  $H_i'$ ,  $H_i^x$ , and  $H_i'$  in  $ZrO_2$  as a function of Fermi level. The black dashed line marks the Fermi level at which the formation energies of  $H_i'$  and  $H_i'$  are equal, which is the defined universal hydrogen level in [2]. (b) Resulted band alignment between  $ZrO_2$  and water (in eV). The energy levels are referenced to vacuum.

To confirm this method, we also compare the resulted electron affinity of  $ZrO_2$  (-3.78 eV) to experimentally-measured values. In Ref [3], electron affinity of -3.41 eV is reported. This experimentally-measured electron affinity yields a valence band offset of -0.34 eV. This offset difference does not change the qualitative conclusions we made regarding the effect of different dopants. To confirm this, we reproduce the electrostatic profiles in Figure 4 in the main article with -0.34 eV valence band offset, as shown in Figure S4. We observe that the total potential drop is decreased by about 0.5 eV across the two sides because of the smaller Fermi level difference on the two sides. This leads to a PZC change of about 2 to the alkali regime.

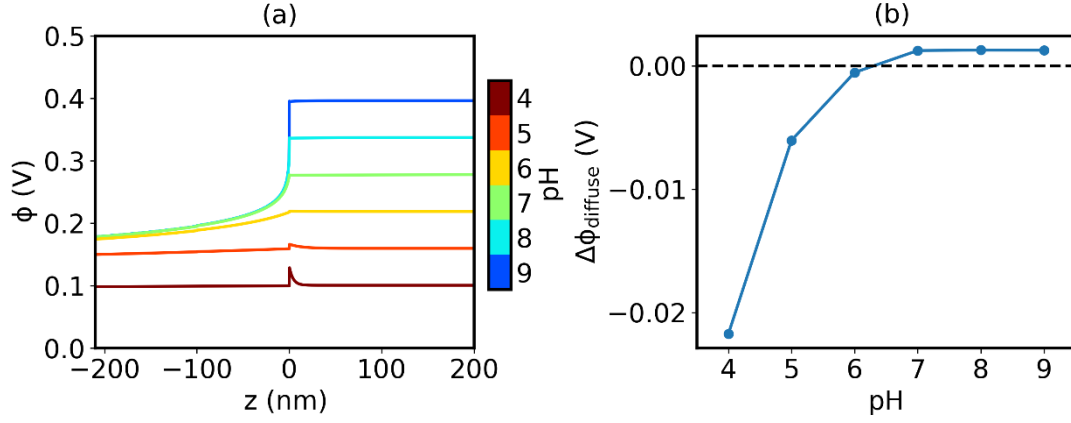


Figure S4. Reproducing Figure 4 in the main article with  $-0.34$  eV valence band offset produced by aligning both bands to vacuum. (a) Electrostatic potential profile with varying pH of water solution. (b) Potential drop in the diffuse layer  $\Delta\phi_{\text{diffuse}}$  as a function of pH. The point where the potential drop reaches zero corresponds to PZC.

### 3. Solution scheme of the continuum model

In this section we give a detailed description of how the continuum level model is solved. In this work, we explicitly considered the Stern layer at water/ $\text{ZrO}_2$  interface, where ions have non-zero adsorption energy. This separates the system into three distinctive regions,  $\text{ZrO}_2$  (region 1), Stern layer of water solution (region 2 ad), and bulk water solution (region 2). We denote the boundary between region 1 and 2 ad as boundary A and the boundary between region 2 and 2 ad as boundary B. In Figure S5(a) we provide the schematics of the whole system. For both boundaries A and B, the continuity of electric displacement field is applied. For boundary A, this continuity constraint is equivalent to global charge neutrality condition, as has been proven in our previous work.[4] For boundary B, this condition is reduced to continuity of electric field because of the assumption of constant dielectric permittivity of water both in the diffuse and the stern layers

In Figure S5(b) we give the notations for the potential in each region. The zero point of potential can be arbitrarily defined. Here we set the potential in bulk  $\text{ZrO}_2$  as 0, and the potential in bulk water as  $\phi_{\text{bulit-up}}$ . The voltage drop in each of the three regions are denoted as  $\Delta\phi_1$ ,  $\Delta\phi_2^{ad}$ , and  $\Delta\phi_2$ . The sum of  $\Delta\phi_1$ ,  $\Delta\phi_2^{ad}$ , and  $\Delta\phi_2$  is equal to  $\phi_{\text{bulit-up}}$ .

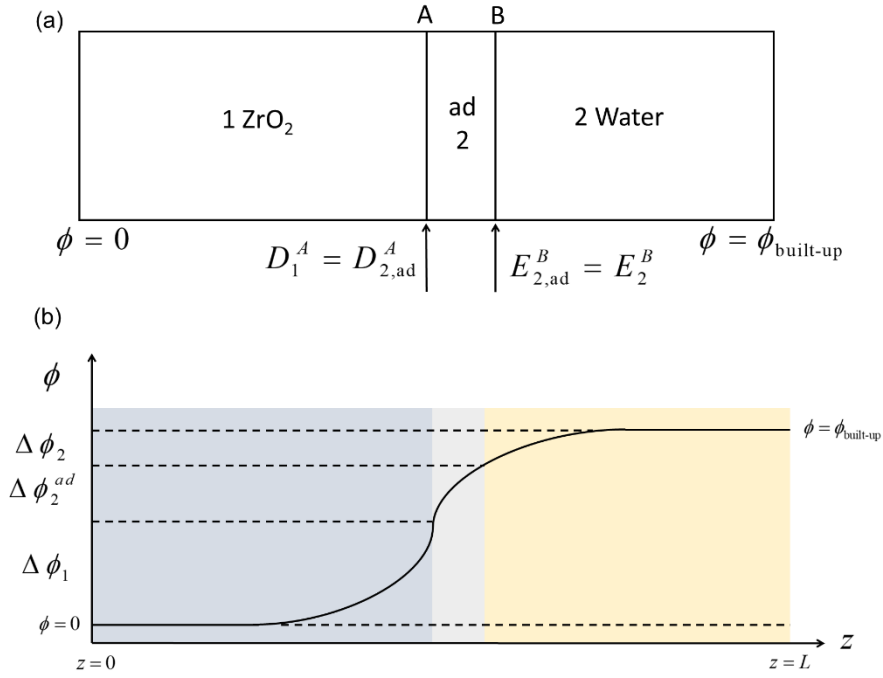


Figure S5. Schematics of the system solved on continuum level. (a) Boundary conditions. (b) Potential drop across each region.

The solution scheme can be designed in multiple ways as long as the final solution satisfies the necessary boundary conditions. In this work, our design goes as follows:

- (1) For a given pH in water and doping concentration in the solid, solve for the bulk equilibrium of water solution and ZrO<sub>2</sub>.  $\phi_{\text{built-up}}$  is determined as the difference in Fermi level on the two sides.
- (2) Give an initial guess of  $\Delta\phi_1$ . Solve Poisson's equation for region 1. Calculate electric fields  $E_1^A$ .
- (3) Give an initial guess of  $\Delta\phi_2^{ad}$ . This also determines  $\Delta\phi_2 = \phi_{\text{built-up}} - \Delta\phi_1 - \Delta\phi_2^{ad}$ .
- (4) Solve Poisson's equation for region 2 ad and region 2. Iterate over  $\Delta\phi_2^{ad}$  until  $E_2^B = E_{2,\text{ad}}^B$  is satisfied.
- (5) Integrate the charge density to get  $\rho_{\text{tot}}$ . If  $\rho_{\text{tot}}$  is approximately equal to zero

within the error range, the problem is solved. If not, go back to step (2) with a new guess of  $\Delta\phi_1$ .

In this work,  $L$  is taken as 8  $\mu\text{m}$ , with 5  $\mu\text{m}$  on the  $\text{ZrO}_2$  side and 3  $\mu\text{m}$  on the water side. The mesh size is set to 1 nm, except for the interfacial core zone, where a mesh size of 0.2  $\text{\AA}$  is used. The linear equations are solved by a direct solver using Cholesky factorization for sparse matrix as implemented in the C++ eigen library.

#### **4. Bulk defect chemistry of doped- $\text{ZrO}_2$**

In previously published results, we have examined the defect chemistry of monoclinic  $\text{ZrO}_2$  thoroughly. [5] Here we include the equilibrium defect concentration profiles (Figure S6) at room temperature and water environment with the same method as in the previous reports. We observe that different from high temperature condition in [5], the dominant hydrogen-related defects are  $\text{H}_{5\text{Zr}}^\bullet$  and  $\text{H}_{2\text{Zr}}''$ , indicating that hydrogen clustering is more favorable under low temperature. In p-type doped case (Fe and Cr),  $\text{H}_{5\text{Zr}}^\bullet$  concentration is promoted and  $\text{H}_{2\text{Zr}}''$  depleted. The opposite is true for n-type doped (Nb) case. Sn exists in  $\text{ZrO}_2$  dominantly in 4+ valence state, therefore does not change the defect chemistry by much as it leads to a neutral substitutional defect.

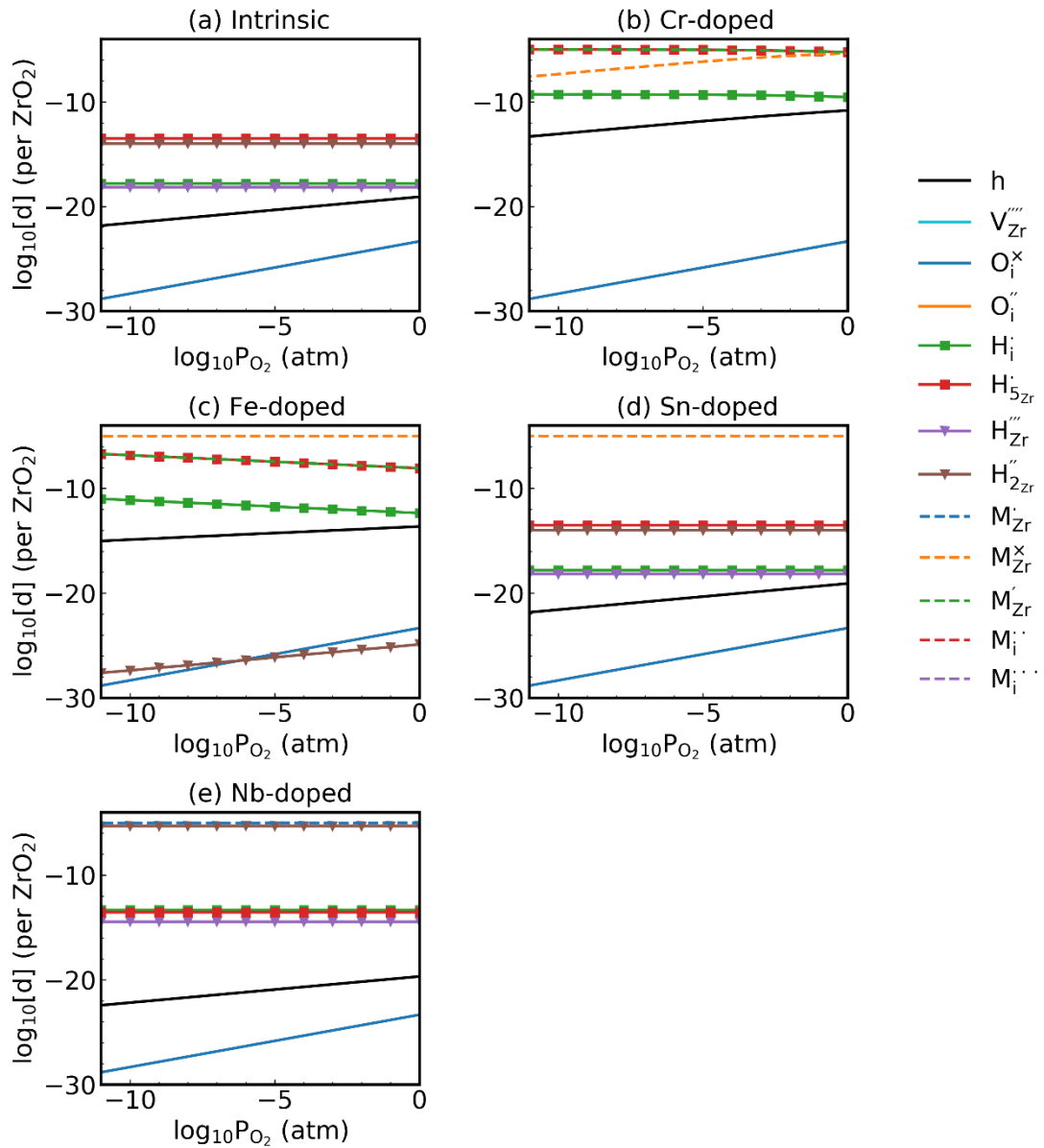


Figure S6. Equilibrium concentration defect concentrations predicted as a function of oxygen partial pressure at 300 K for (a) intrinsic ZrO<sub>2</sub>, (b) Cr-doped ZrO<sub>2</sub>, (c) Fe-doped ZrO<sub>2</sub>, (d) Sn-doped ZrO<sub>2</sub>, and (e) Nb-doped ZrO<sub>2</sub>. For all doped cases, dopant concentrations are fixed to 10 ppm.

## 5. Electrostatic profile of doped-ZrO<sub>2</sub>/water interface with varying pH

In the main article, we studied the defect redistribution profile of differently-doped ZrO<sub>2</sub> interfacing with water. Here we look closely into the electrostatic profiles with varying pH, as shown in Figure S7. Comparing to undoped case in Figure 4, the

electrostatic profile of Sn-doped  $\text{ZrO}_2$ /water interface does not change because Sn exist dominantly in 4+ state. The two acceptor dopants, Cr and Fe, decreases the Fermi level of  $\text{ZrO}_2$  and therefore increases the Fermi level difference between  $\text{ZrO}_2$  and water. The potential differences on the two sides are increased. Nb has the reverse effect by increasing the Fermi level of  $\text{ZrO}_2$  and thus decrease the built-in potential.

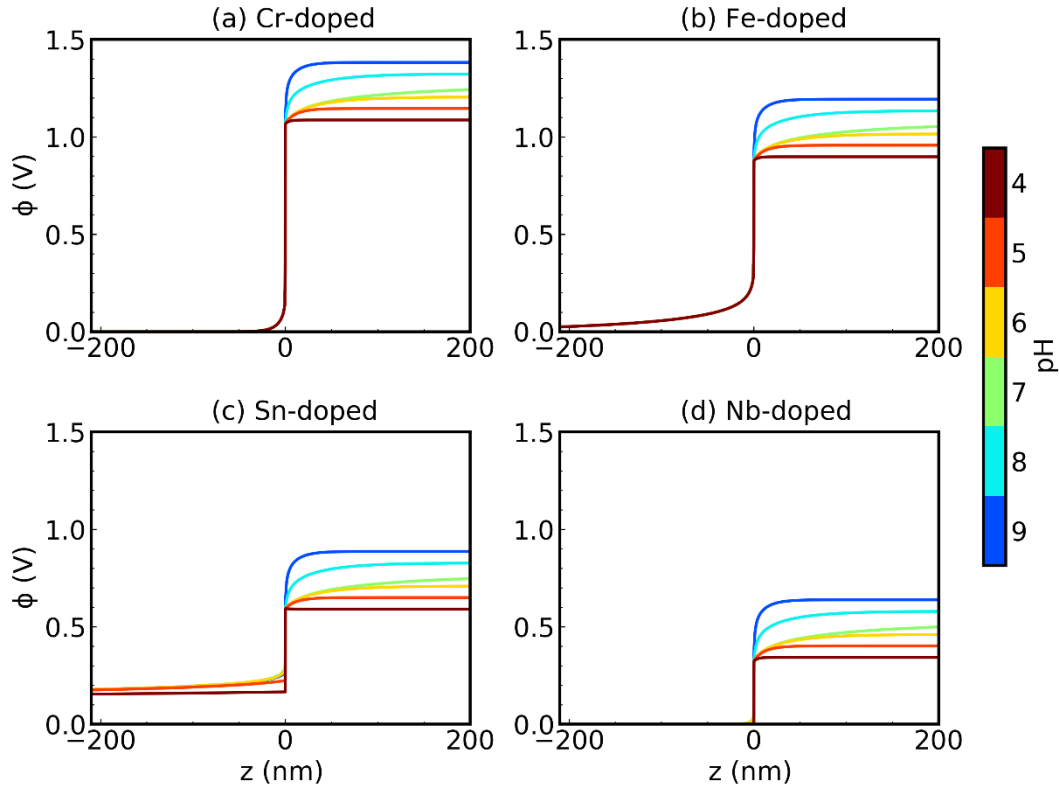


Figure S7. Electrostatic potential profiles across doped- $\text{ZrO}_2$ /water interface at varying pH. (a) Cr-doped, (b) Fe-doped, (c) Sn-doped and (d) Nb-doped. Dopant levels are fixed to 10 ppm in bulk. The profiles at pH = 7 correspond to Figure 5 in the main article.

## 6. Effect of varying defect concentration

Throughout the manuscript we studied dopants with a fixed concentration of 10 ppm in bulk, which is typical in  $\text{ZrO}_2$  grown natively on zirconium alloy. In Figure S8, Figure S9, and Figure S10 we show the defect concentration comparison with varying concentration of Cr, Fe, and Nb. Generally, we observe a trend that the effects of different dopants decrease with smaller doping concentrations and gradually converge to intrinsic level.

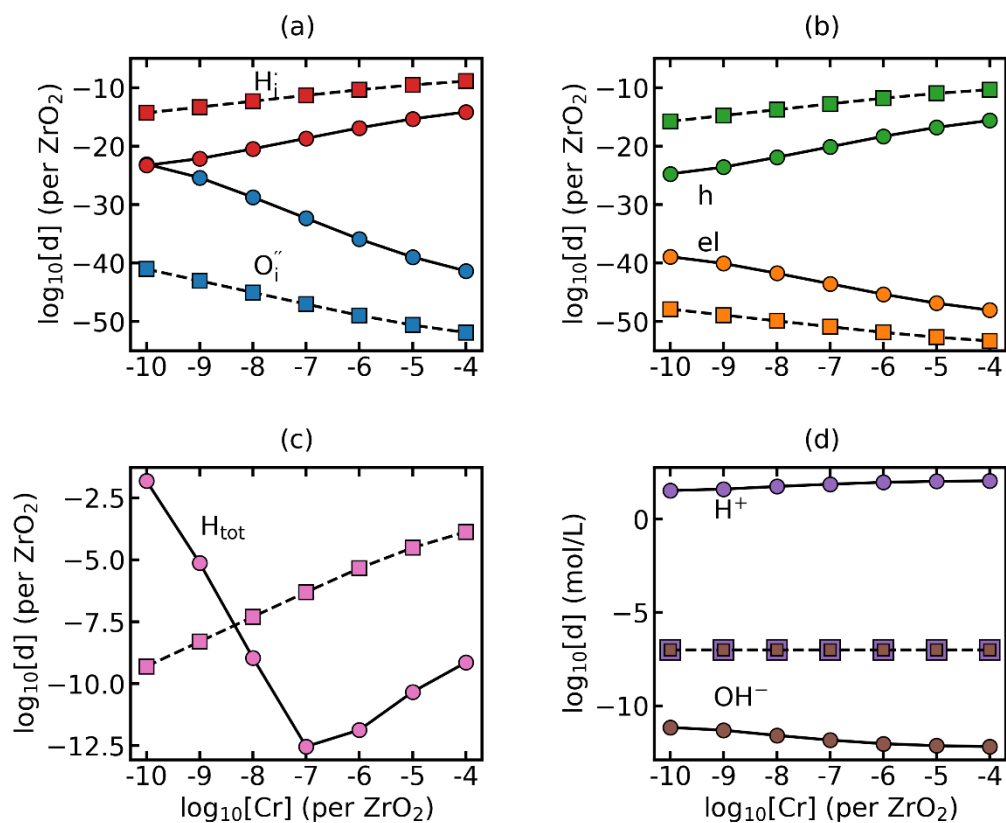


Figure S8. Comparison of surface (represented by solid line and circles) and bulk concentration (represented by dashed line and squares) of species related to oxygen and hydrogen incorporation as a function of Cr dopant concentration in  $ZrO_2$ . (a)  $H_i^+$  and  $O_i^{\bullet}$ , (b) free electrons and holes, (c) total concentration of hydrogen, and (d)  $H^+$  and  $OH^-$  in bulk water and at surface. All calculations are done at pH = 7.

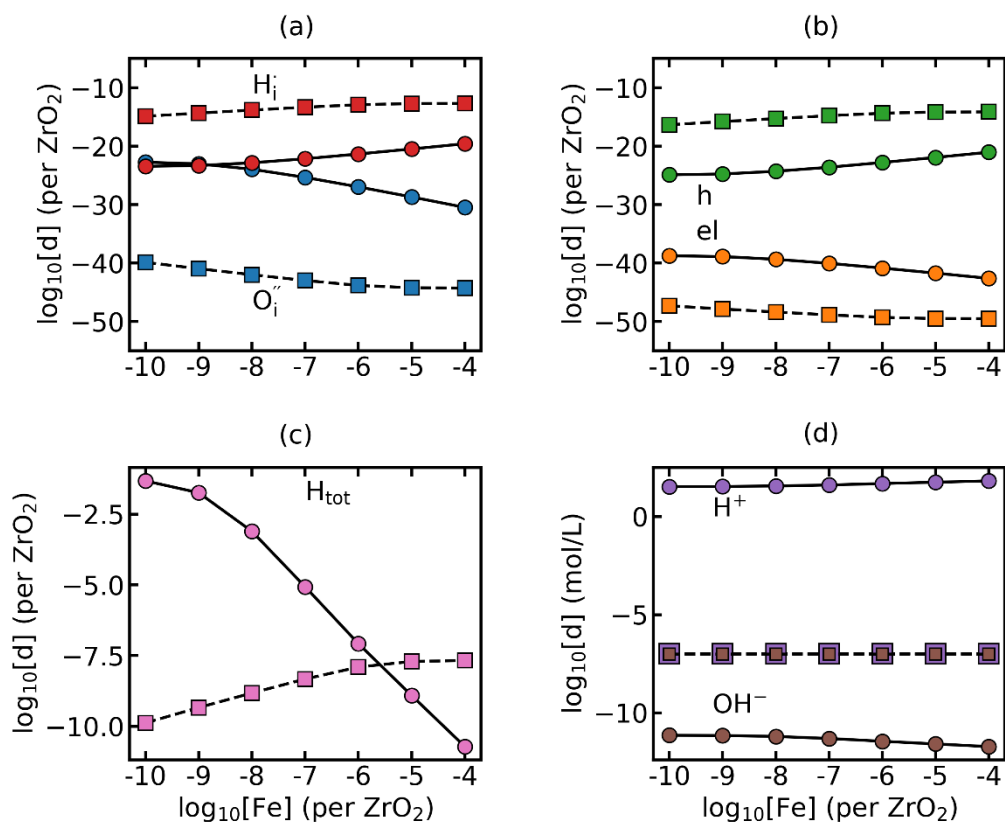


Figure S9. Comparison of surface (represented by solid line and circles) and bulk concentration (represented by dashed line and squares) of species related to oxygen and hydrogen incorporation as a function of Fe dopant concentration in ZrO<sub>2</sub>. (a) H<sub>i</sub>' and O<sub>i</sub>'', (b) free electrons and holes, (c) total concentration of hydrogen, and (d) H<sup>+</sup> and OH<sup>-</sup> in bulk water and at surface. All calculations are done at pH = 7.

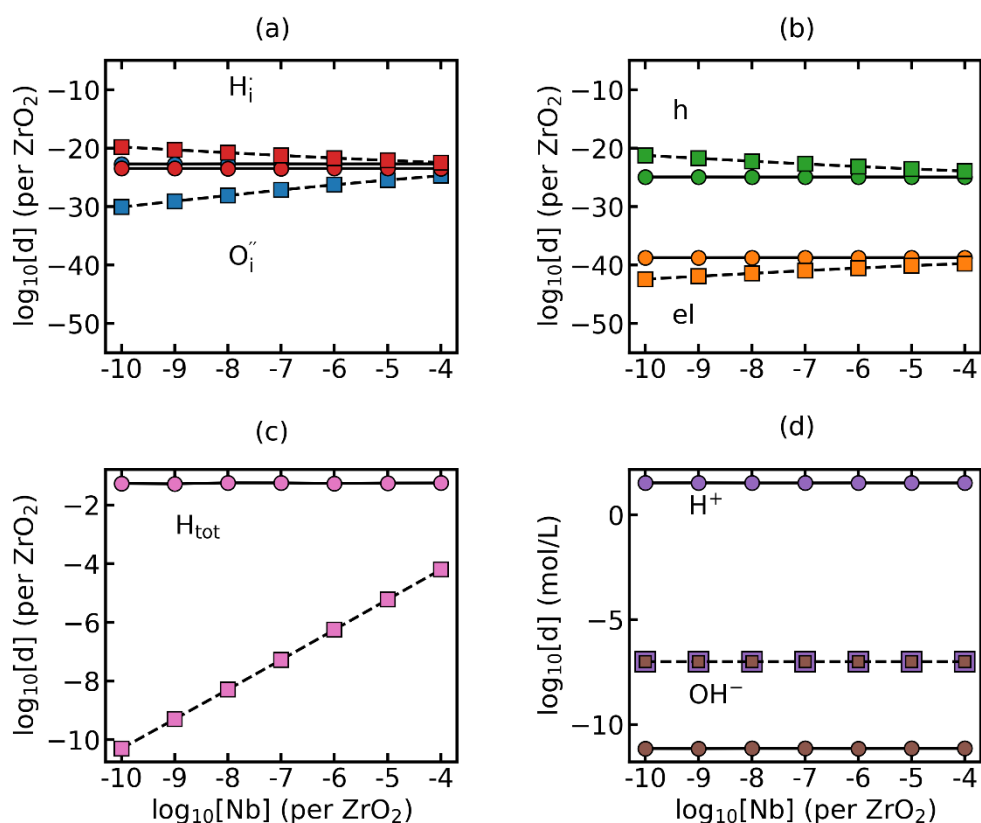


Figure S10. Comparison of surface (represented by solid line and circles) and bulk concentration (represented by dashed line and squares) of species related to oxygen and hydrogen incorporation as a function of Nb dopant concentration in ZrO<sub>2</sub>. (a) H<sub>i</sub>' and O<sub>i</sub>'', (b) free electrons and holes, (c) total concentration of hydrogen, and (d) H<sup>+</sup> and OH<sup>-</sup> in bulk water and at surface. All calculations are done at pH = 7.

## References

- [1] M. Todorova and J. Neugebauer, *Physical Review Applied* **1** (2014).
- [2] C. G. Van de Walle and J. Neugebauer, *Nature* **423**, 626 (2003).
- [3] *American Mineralogist* **85**, 543 (2000).
- [4] J. Yang, M. Youssef, and B. Yildiz, *Physical Chemistry Chemical Physics* **19**, 3869 (2017).
- [5] M. Youssef, M. Yang, and B. Yildiz, *Physical Review Applied* **5** (2016).